

# A Generalizable Model for Fault Detection in Offshore Wind Turbines Based on Deep Learning

Soorena Salari and Nasser Sadati\*, *Member, IEEE*

**Abstract**— This paper presents a new deep learning-based model for fault detection in offshore wind turbines. To design a generalizable model for fault detection, we use 5 sensors and a sliding window to exploit the inherent temporal information contained in the raw time-series data obtained from sensors. The proposed model uses the nonlinear relationships among multiple sensor variables and the temporal dependency of each sensor on others that considerably increases the performance of fault detection model. A 10-fold cross-validation is used to verify the generalization of the model and evaluate the classification metrics. To evaluate the performance of the model, simulated data from a benchmark floating offshore wind turbine (FOWT) with supervisory control and data acquisition (SCADA) are used. The results illustrate that the proposed model would accurately disclose and classify more than 99% of the faults. Moreover, it is generalizable and can be used to detect faults for different types of systems.

**Index Terms**— Fault detection, fault classification, offshore wind turbines, convolutional LSTM, deep learning.

## I. INTRODUCTION

IN recent years, as a result of the global warming phenomena, wind turbines have played an important role in generating reliable, cost-effective, and pollution-free energy. Although the complex design, expensive platforms, long-distance cabling, and maintenance cost have made the electricity production cost of FOWTs three times higher than that of onshore ones, FOWTs are more advantageous owing to much steadier winds at sea, less noise pollution, and less negative impact on the environment. Moreover, the development of offshore wind energy requires careful design, planning, and installation of offshore wind farms, where their reliability can be ensured using efficient fault detection model.

Actuator and sensor faults are common fault types that mostly occur in wind turbines. They usually arise due to mechanical and electrical reasons in most subsystems of the FOWTs, either weakly or severely. Based on two fault detection methods, i.e. model-based and data-driven methods, various techniques for fault detection in wind turbines have been proposed. Model-based methods rely on exact and highly reliable models, while wind turbines work under harsh environments and are subjected to large wind fluctuations. Therefore, we use data-driven methods, where the faulty situations can be detected in minimal time.

Data-driven methods are increasingly used in fault detection of wind turbines as a result of the difficulty in system modeling and, moreover, the availability of data.

Nowadays deep learning is employed in various applications, from computer vision to economics. Unlike shallow networks, deep learning can deal with massive data sets without using feature selection, and it has had a breakthrough in certain applications [1]. In [2] and [3], the principal information on fault diagnosis and condition monitoring of wind turbines have been investigated. A comprehensive review in wind turbine condition monitoring is also given in [4]. A fault detection model based on image texture analysis using statistical machine learning methods such as K nearest neighbors (KNN), bagged trees, and decision tree is presented in [5] with more than 80% accuracy. A sliding window in the data preprocessing and denoising autoencoder with PCA for fault detection of wind turbines is suggested in [6]. In [7], a fault detection and classification model using long short-term memory (LSTM) employing sensor data generated from a real wind turbine is presented. A fault detection model using a random forest classifier with actuator and sensor data for offshore wind turbines is also presented in [8]. An ensemble of some statistical models like support vector machine (SVM) and multi-layer perceptron (MLP) also is used for fault detection in offshore wind turbines [9].

This paper presents a novel approach for fault detection based on deep learning. The main features of the proposed method can be summarized as follows:

- 1) We suggest 2 convolutional neural networks (CNNs), and a convolutional LSTM (ConvLSTM) that considers nonlinear correlation among multivariate sensor data. To the best of our knowledge, this paper is the first to propose ConvLSTM for fault detection in offshore wind turbines.
- 2) A sliding window is considered for inherent time dependency present in the data set. Thus, the proposed models use new data that contains current and past relationships among sensors, which increases the accuracy of fault detection.
- 3) Sensors are costly components in offshore wind turbines. Therefore, unlike other fault detection models that use 13 and 8 sensors for fault detection

in offshore wind turbines [5], [7], we only use 5 sensors and improve the fault detection accuracy.

The data set is derived from the SCADA developed by the National Renewable Laboratory (NREL) for fault detection and fault-tolerant control of a benchmark MW-scale wind turbine [10], [11]. This benchmark provides the same model for all researchers to evaluate their fault detection models in the presence of common faults. Thus, after gathering data and preparing labels, we preprocess the data. Then, we train and test the models with 10-fold cross-validation. Finally, simulation results are evaluated by various machine learning metrics to show their performance in classifying faulty cases from the normal ones.

## II. BENCHMARK MODEL

In this section, we introduce the benchmark model used for simulating and collecting data, as proposed in [11]. This benchmark model is a 3-bladed horizontal axis variable speed wind turbine consisting of a fully coupled converter, which its rated power is 5 MW. The aim of this benchmark model is to provide a base model with which all researchers can compare their results. This benchmark is based on software developed by NREL called fatigue, aerodynamics, structures, and turbulence (FAST), which is an aeroelastic wind turbine simulator [12]. With this powerful software, researchers can quickly simulate the wind turbine structural behavior with up to 24 degrees of freedom. In this paper, FAST numerical simulations of the NREL 5-MW offshore wind turbine are accomplished. The characteristics of this turbine can be found in Table I [13]. Wind data sets are also generated by TurbSim [14], to make the methodology more realistic. The wind has the following characteristics:

- 1) Kaimal turbulence model with 10% intensity,
- 2) Mean speed of 18.2 m/s at the hub height.

Fig. 1 shows sample of a generated wind profile with duration of 600 s.

TABLE I  
THE NREL 5-MW WIND TURBINE CHARACTERISTICS [13]

Information	Measure
Rated power	5 MW
Number of blades	3
Height of tower	87.6 m
Gearbox ratio	98
Rotor diameter	126 m
Cut-in, rated, cut-out wind speed	3 m/s, 11.4 m/s, 25 m/s
Nominal generator speed	1173.7 rpm

### A. Generator – converter actuator model

The dynamic equation of a generator coupled with a converter is as follows [1]:

$$\dot{\tau}_g + \alpha_g \tau_g(t) = \alpha_{gc} \hat{\tau}_{gr}(t), \quad (1)$$

where  $\hat{\tau}_{gr}$  is the generator torque reference signal,  $\tau_g$  is the generator torque, and  $\alpha_{gc}$  is the converter model parameter.

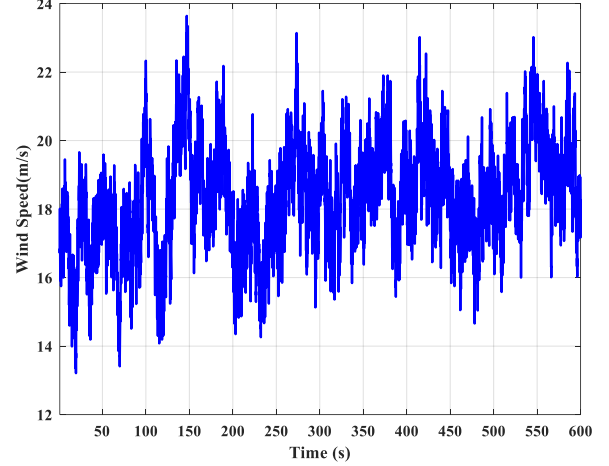


Fig. 1. A generated wind profile.

Also, the nominal value of  $\alpha_{gc}$  is 50. The generator output power is given by:

$$P_g(t) = \eta_g \omega_g(t) \tau_g(t), \quad (2)$$

where the nominal value of  $\eta_g$  is 0.98.

### B. Pitch angle actuator model

The dynamics of a hydraulic pitch angle actuator is as follows:

$$\ddot{\beta} + 2\zeta \omega_n \dot{\beta} + \omega_n^2 \beta = \omega_n^2 \hat{\beta}_c, \quad (3)$$

where  $\omega_n$  is the natural frequency and  $\zeta$  is the damping coefficient. Equation (3) corresponds to all three blades. The nominal values of  $\zeta$  and  $\omega_n$  are 0.7 and 11.11 rad/s, respectively [11].

### C. Baseline controller

The 5-MW reference wind turbine has both collective pitch controller and torque controller, where their input is generator's speed. These baseline controllers are commonly used among researchers for the purpose of comparison [15]–[17]. To reduce the high-frequency dynamics of the control system in the gain-scheduling PI (GSPI) controller, a low-pass filter is used for generator speed [13].

The baseline torque controller is given by:

$$\tau_{g,r}(t) = \frac{P_{ref}(t)}{\hat{\omega}_g(t)}, \quad (4)$$

where  $\hat{\omega}_g$  is the output of the low-pass filter, and  $P_{ref}$  represents the reference power.

A baseline collective pitch controller is used as a GSPI controller with generator speed as its input [13]. The

nonlinearities of the wind turbine are compensated by changing the controller's gains. The controller is given by:

$$\beta_c = K_p(t) \left( \hat{\omega}_g(t) - \omega_{gr}(t) \right) + K_i(t) \int_0^t (\hat{\omega}_g(t) - \omega_{gr}(t)) dt, \quad (5)$$

where  $\omega_{gr}$  is the generator speed reference, and  $\beta_c$  represents the pitch angle set point.

#### D. Data set

In this section, we present in details the simulated data set used in this work for training and evaluating the obtained model. All the sensors used in the benchmark model appear in Table II [11]. These sensors, which cover every part of a turbine, are typically used in the MW-scale commercial wind turbines.

In the fault detection phase, 140 simulations for healthy cases and 40 simulations for each fault have been carried out. The sampling frequency is 80 Hz in each simulation. Therefore, we have 420 cases with 13 variables in our data set.

The more sensors deployed in a given system, the more we need to spend; hence, reducing the number of sensors is necessary. We use backward feature selection [18] to find out the importance of each feature. After observing the impact of eliminating each sensor, we have selected only 5 sensors out of 13 sensors and use them in our reduced data set. Our selected sensors are: generator torque, rotor speed, and all three pitch angles.

#### E. Fault scenarios

Wind turbines are subjected to different types of fault conditions. Inspired from [10], [11], the most often occurring faults in a wind turbine are tabulated in Table III.

As mentioned earlier, we use both sensor faults and actuator faults. It should be noted that, since the pitch and torque actuators play a vital role in wind turbine operation, and their failure can cause the whole system to fail, we consider these actuators. In Table III, faults 1, 2, and 3 are the pitch actuator's faults which occur due to hydraulic leakage, pump wear, and high air content [19]. On the other hand, as stated in [20] and [21], some sensor faults are more common and important compared to other sensor faults. For this reason, we choose faults 4, 5 and 6 in our case study. These latter ones could be electrical or mechanical and appear to be due to wrong gain and sensor saturation. Faults 5 and 6 could affect the baseline controller, and the pitch position. Finally, the torque actuator fault (fault 7) could appear because of wrong initialization of the converter or manufacturing failures.

### III. FAULT DETECTION WITH DEEP LEARNING

To the best of authors' knowledge, this paper is the first to propose a new generalizable models to detect faults in offshore wind turbines based on deep learning. In the following, we present our new deep learning approach.

#### A. Recurrent neural networks

A recurrent neural network (RNN) is a class of neural networks that has feedback and hidden states. Recurrent neural

TABLE II  
AVAILABLE SENSORS ON A MW-SCALE INDUSTRIAL TURBINE [11]

Number	Sensor type	Units
1	Rotor speed	rad/s
2	Generator torque	Nm
3	First pitch angle	deg
4	Second pitch angle	deg
5	Third pitch angle	deg
6	Electrical power	kW
7	Generator speed	rad/s
8	Acceleration of fore-aft movement at the tower bottom	m/s <sup>2</sup>
9	Acceleration of side-to-side movement at the tower bottom	m/s <sup>2</sup>
10	Acceleration of fore-aft movement at the mid-tower	m/s <sup>2</sup>
11	Acceleration of side-to-side movement at the mid-tower	m/s <sup>2</sup>
12	Acceleration of fore-aft movement at the top of the tower	m/s <sup>2</sup>
13	Acceleration of side-to-side movement at the top of the tower	m/s <sup>2</sup>

TABLE III  
FAULT SCENARIOS

Fault	Type	Description
1	Pitch actuator	High air content ( $\zeta = 0.45$ and $\omega_n = 5.73$ rad/s)
2	Pitch actuator	Pump wear parameters ( $\zeta = 0.75$ and $\omega_n = 7.27$ rad/s)
3	Pitch actuator	Hydraulic leakage ( $\zeta = 0.9$ and $\omega_n = 3.42$ rad/s)
4	Generator speed sensor	Gain factor (1.2)
5	Pitch angle sensor	Fixed value (10 deg)
6	Pitch angle sensor	Fixed value (5 deg)
7	Torque actuator	Offset value (2000 Nm)

networks have a wide variety of applications from image processing to speech and natural language processing [22]. The output of a hidden state at a specific time depends on previous times and it is given by times and it is given by

$$h(t) = f(W_{hh}h(t-1) + W_{xh}x(t)), \quad (6)$$

where  $W_{hh}$  and  $W_{xh}$  are the learnable parameters,  $x(t)$  is the input at time instant  $t$ ,  $h(t-1)$  is a hidden state at time  $t-1$ , and  $f$  is an activation function like tanh. The output of an RNN is given by:

$$y = W_{yh}h(t). \quad (7)$$

Similar to ordinary neural networks, recurrent neural networks suffer from vanishing and exploding gradients. To update each of the weights in the backpropagation algorithm, we use their gradients. To compute the gradients, the chain rule is employed as follows [23]:

$$\frac{\partial L_j}{\partial W} = \sum_{k=1}^j \frac{\partial L_j}{\partial h_k} \frac{\partial h_k}{\partial W}, \quad (8)$$

where  $W$  represents the network weight matrix,  $L$  represents the loss function, and  $k$  is the layer number. We also use the chain rule to compute  $\partial L_j / \partial h_k$ , and then rewrite (8) as follows:

$$\frac{\partial L_j}{\partial W} = \sum_{k=1}^j \frac{\partial L_j}{\partial y_j} \frac{\partial y_j}{\partial h_k} \frac{\partial h_k}{\partial W}. \quad (9)$$

Because each state is related to previous states involving nonlinear equations, we calculate  $\partial h_j / \partial h_k$  as follows:

$$\frac{\partial h_j}{\partial h_k} = \prod_{m=k+1}^j \frac{\partial h_m}{\partial h_{m-1}}. \quad (10)$$

Now by combining (9) and (10), we obtain:

$$\frac{\partial L_j}{\partial W} = \sum_{k=1}^j \frac{\partial L_j}{\partial y_j} \frac{\partial y_j}{\partial h_j} \left( \prod_{m=k+1}^j \frac{\partial h_m}{\partial h_{m-1}} \right) \frac{\partial h_k}{\partial W}. \quad (11)$$

The nonlinear function for each state of the equation, which is related to previous states, is usually a tanh or ReLU activation function, and based on (10), the nonlinear functions are multiplied together. If the gradient is less than 1, after many multiplications in (10), based on (11) the value of gradient approaches zero and vanishes, which in turn prevents the weights from updating their values. Furthermore, if the gradient is more than 1, after many multiplications in (10), based on (11) the value of gradient will become unlimited and explodes. We should remark that such a gradient computation requires a lot of memory [22].

### B. Convolutional neural networks

Convolutional neural networks (CNNs) makes a noteworthy improvement in image processing, speech processing, and neuroscience. This progress is caused by a mixture of algorithmic developments and accessing to large amounts of data and computer resources [24]. CNN has two main layers: the convolutional layer and the pooling layer. The first layer is the core of the network, where the convolution operation is performed. The convolution operation is calculated as follows:

$$s(t) = \int x(a) w(t-a) da, \quad (12)$$

where  $x$ ,  $w$  and  $s$  represent the input, kernel, and the output, respectively. In convolutional network terminology, the output is known as feature map. Kernels are trainable weights and optimized during the training stage with backpropagation. The second layer is the pooling layer, which reduces the size of the feature map. As a result of this size reduction, in the next convolutional layer of the network, the kernels with lower size are needed and consequently the number of parameters for training and the amount of computation in the network are decreased. After convolution layer, the pooling layer is used for

taking subsamples from the feature map, which has been produced by the convolutional layer. The subsample operation usually takes the maximum or average of the feature map. This layer helps the network to recognize patterns in data set and makes the network more robust against rotation and scaling. By these two layers, CNN uses local features and nonlinear transformation, and it can also extract distinctive patterns by learning from data.

### C. Long short-term memory

The LSTM is a kind of recurrent neural network that relates to time series, and it can solve the vanishing gradient as well as exploding gradient problem [25]. Fig. 1S in the supplementary material shows the LSTM structure.

The LSTM equations are given as follows:

$$z_t = g(W_z x_t + R_z y_{t-1} + b_z) \quad (13)$$

$$i_t = \sigma(W_i x_t + R_i y_{t-1} + p_i \odot c_{t-1} + b_i) \quad (14)$$

$$c_t = z_t \odot i_t + c_{t-1} \odot f_t \quad (15)$$

$$f_t = \sigma(W_f x_t + R_f y_{t-1} + p_f \odot c_{t-1} + b_f) \quad (16)$$

$$y_t = h(c_t) \odot o_t \quad (17)$$

$$o_t = \sigma(W_o x_t + R_o y_{t-1} + p_o \odot c_t + b_o), \quad (18)$$

where  $z_t$  is the input block,  $i_t$  is the input gate,  $c_t$  is the memory cell,  $f_t$  is the forget gate,  $y_t$  is the output and  $o_t$  is the output gate. Also  $W_z$ ,  $W_i$ ,  $W_f$ , and  $W_o$  denote the input weight matrices for the input gate, forget gate and the output gate;  $p_i$ ,  $p_f$ , and  $p_o$  are the peephole weight matrices;  $R_z$ ,  $R_i$ ,  $R_f$ , and  $R_o$  are recurrent weight matrices;  $b_z$ ,  $b_i$ ,  $b_f$ , and  $b_o$  are bias weight matrices; and the operator  $\odot$  means element-wise multiplication. In addition,  $\sigma$ ,  $g$  and  $h$  represent the logistic functions, usually considered as sigmoid or tanh activation functions. The memory cell is an important part of an LSTM network and can replace matrix multiplication with a first-order recursive equation. Therefore, vanishing and exploding gradients are eliminated and the model can be trained well [26].

### D. ConvLSTM

ConvLSTM replaces matrix multiplication with convolution operation at each gate in the LSTM cell [27]. Unlike recurrent neural networks, LSTM learns long-term dependencies by assigning the forget gate to 1. In addition, when the forget gate is set to 1 during backpropagation, the derivative is always 1 and the gradient of the memory cell does not vanish. In this paper, we use ConvLSTM to benefit its power in confronting the sequential data.

### E. Data preprocessing

One of the challenging problems in fault detection is reducing the time needed for fault detection and accommodation. The offshore wind turbines are exposed to difficult phenomena such as wind and waves, and therefore, immediate fault detection is essential for damage prevention.

In this paper, we use an overlapping sliding window with a length of only 200 samples (2.5 s), where each sample is a 2-D matrix whose first axis is time and the second axis is the sensor measurement. In the previous work, the whole signal length of 600 s is considered [5].

#### F. Network architecture

Our first proposed model is constructed by CNN, as shown in Fig. 2S in the supplementary material. It consists of 3 forward ways. In each part of the network, we have a convolutional layer with 100, 90, and 80 filters with kernel sizes of  $1 \times 5$ ,  $7 \times 5$ , and  $20 \times 5$ , respectively. The output of all convolutional layers is followed by a LeakyReLU activation function and a batch normalization regularizer [28]. We use concatenation of 3 convolution layers that are followed by an MLP for classification, where each layer is used for a specific purpose. For example, when we use a filter with kernel size of  $20 \times 5$ , the relevance of each of 20 sample times with 20 nearby sample times is calculated. Because we use the concatenation of these outputs, our model is an example of the ensemble learning algorithm of convolutional layers. The model training is performed by 50 epochs, batch size of 32, and an Adam optimizer [29].

The second proposed model constructed by CNN is shown in Fig. 3S in the supplementary material. This model consists of the following components: 8 hidden layers (convolution and dense layers), where each convolution and dense layer is followed by an activation function. The first two convolutional layers contain 10 filters, kernel size of 10, and ReLU activation functions. Thus, a batch normalization layer and 2 convolutional layers with 20 filters and kernel size of 10 are added. After convolutional layers, dropout regularization only keeps 50% of the nodes for training. Max pooling is added to the model to reduce the dimension of data and avoid overfitting problem. Finally, the model is followed by a dense layer for classification. In addition, model training is performed by 50 epochs, batch size of 32, and an Adam optimizer.

The proposed ConvLSTM for fault detection is shown in Fig. 2. We use ConvLSTM to benefit its power in working with sequential data and the convolution simultaneously. Each sample is a  $125 \times 5$  matrix, and because of the input dimension in the input layer of ConvLSTM, each input has been reshaped to a 4-D matrix with  $5 \times 1 \times 25 \times 5$  dimensions. Our final ConvLSTM is formed by four ConvLSTM layers with 32, 32, 64, and 64 filters with kernel sizes of  $1 \times 5$ ,  $1 \times 5$ ,  $1 \times 3$ , and  $1 \times 3$  respectively, having ReLU activation functions, and two fully connected layers. To reduce the overfitting problem and increase the network generalization, the ConvLSTM is followed by a batch normalization layer [28]. We finally have our output node connected to the dense layers to be exploited for classification algorithm. Furthermore, the model is trained with 300 epochs with a batch size of 256. In addition, the learning rate of Adam optimizer is set to 0.005. Each ConvLSTM layer has a precise meaning, that is when we use a filter with a size of  $1 \times 5$ , the connection with other sensor samples will be observed every 5 samples.

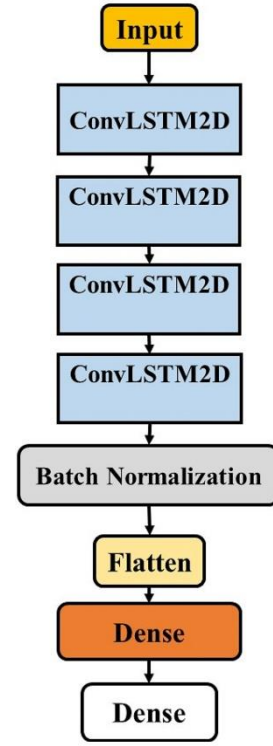


Fig. 2. The proposed ConvLSTM for fault detection.

#### IV. RESULTS AND DISCUSSION

In this section, the simulation results and discussion are presented. The proposed fault detection models are implemented using Keras library with Python 3.6 support [30] and NVIDIA Tesla K80 model GPU. After training the deep learning models, we use some metrics to evaluate and compare the performance of the proposed models with each other. The selected metrics are as follows [31]–[33] :

- 1) Accuracy =  $(TP + TN) / (TP + TN + FP + FN)$
- 2) Precision =  $TP / (TP + FP)$
- 3) Recall =  $TP / (TP + FN)$
- 4) F-score =  $2TP / (2TP + FP + FN)$
- 5) Receiver operating characteristics (ROC)
- 6) Area under the ROC curve (AUC)
- 7) Confusion matrix,

where TP stands for true positive (correctly classified), TN stands for true negative (correctly classified), FP stands for false positive (incorrectly classified) and FN stands for false negative (incorrectly classified). More information about accuracy, precision, recall, F-score, ROC, AUC and confusion matrix can be found in [23], [34], [35].

Table IV presents the results of 10-fold cross-validation. The confusion matrices for models are also shown in Figs. 2, 3 and 4. Moreover, the ROC curves for models are shown in Figs. 4S, 5S and 6S in the supplementary material. In ROC curves, class 0 is for normal samples, while other classes (classes 1-7) are for fault samples. When working with time series data, because the patterns change over time, the models should demonstrate a good performance at all times. The network architecture and

parameters of the models are tuned by trial and error, based on practical knowledge and experience.

The t-distributed stochastic neighbor embedding (t-SNE) method [36], which represents a nonlinear dimensionality reduction technique, is employed for layer representation of the proposed ConvLSTM. During the training of the ConvLSTM, the output of each layer represents the higher quality feature. This representation illustrates how ConvLSTM captures time dependencies. As we can see from Fig. 6, after the first ConvLSTM layer, faults 4, 5 and 6 become discernible, which denotes that these classes of faults are more comfortable to detect than others. After the fourth ConvLSTM layer, fault 7 and normal cases can be distinguished from other classes, and after 50 hidden units, fault 3 becomes separable. Finally, after the fully connected (FC) layer, all classes are separable, and that confirms the results of the ConvLSTM model. Faults 1, and 2 (pitch actuator's faults) represent the most challenging faults, which distinguish from each other in the FC layer. On the other hand, from the first ConvLSTM layer (top left in Fig. 6) to the second ConvLSTM layer (bottom left of Fig. 6), it can be seen that by increasing the size of the input signal, the classes become more separable, which confirm the importance of time dependencies for classification. Thus, the ConvLSTM model considers time dependencies well.

As we indicated earlier, the proposed models can predict the test samples well. However, the CNN models are not able to detect faults 1, 2, and 3, whereas the ConvLSTM correctly detects all faults. In [5], samples from 13 sensors, each with a

TABLE IV  
RESULTS OF EACH MODEL

Model	Accuracy	Precision	Recall	F-score	AUC
First CNN	70.1%	0.558	0.61	0.581	0.95
Second CNN	70.6%	0.562	0.62	0.589	0.95
ConvLSTM	99.4%	0.994	0.994	0.994	1

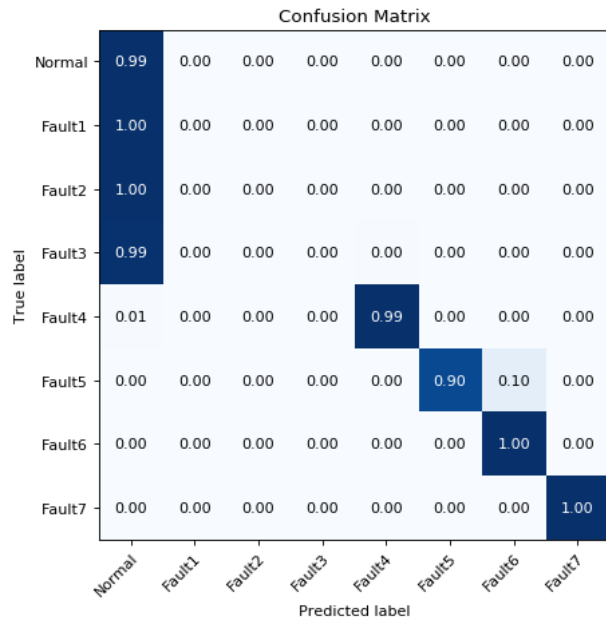


Fig. 3. The confusion matrix for the first CNN.

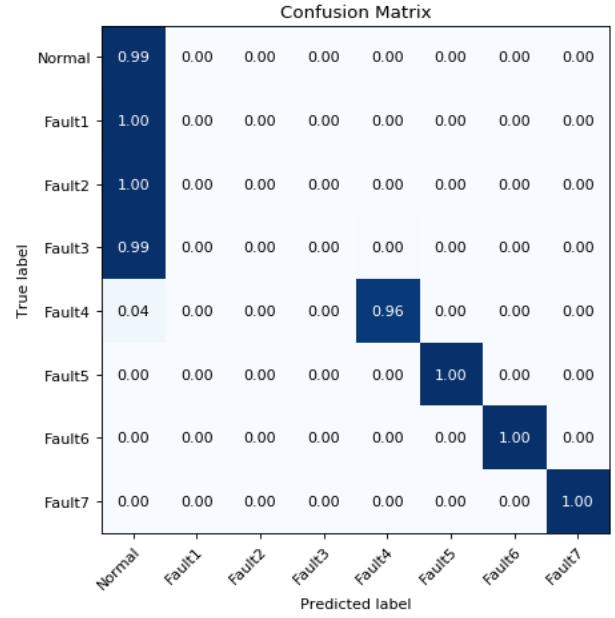


Fig. 4. The confusion matrix for the second CNN.

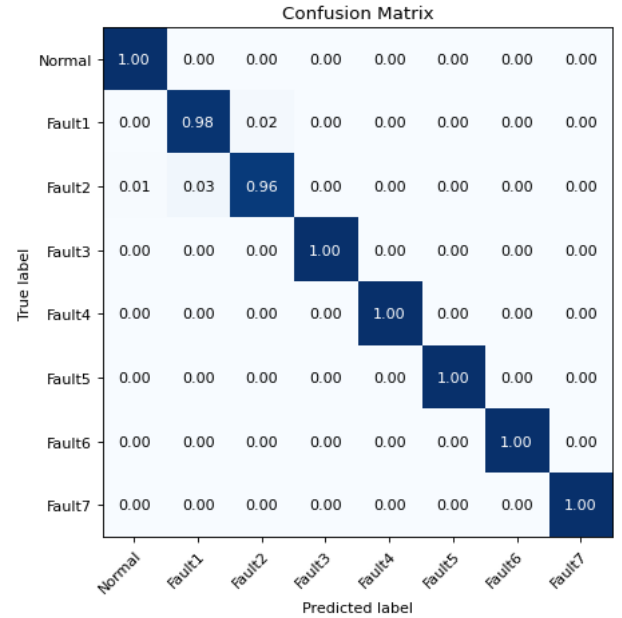


Fig. 5. The confusion matrix for the ConvLSTM.

length of 600 s is transformed to grayscale images and used for feature extraction. After feature extraction, several classifiers are used for fault classification. It is shown that with 80% accuracy, the bagged trees provide an improvement over other classifiers [5]. Compared to the previous approach [5], the proposed ConvLSTM exhibits 99.4% accuracy, by only using 5 sensors instead of 13. It is also worth mentioning that every one of our samples has a length of only 1.5 s, which is much shorter than the input length reported by [5]. As a result, our fault detection model can detect faults much faster than the existing models. In other words, when the input length of the fault detection model is more, it needs more time to wait for samples, and hence it acts slower than the other models with



shorter input lengths. By using only 5 sensors for fault detection and classification, we can reduce the cost of operation of offshore wind turbines.

## V. CONCLUSION

In recent years, different state-of-the-art deep learning methods have demonstrated good performance in various applications. In this paper, to optimally take advantage of the impressive performances of RNN and LSTM, we proposed three different deep learning models, including two CNNs and one ConvLSTM for fault detection in offshore wind turbines. The obtained results indicate that our proposed ConvLSTM achieves an average accuracy of 99.4% over all faults, and it outperforms the proposed CNNs in this study and also the previous models using the same data set. The advantages of our proposed ConvLSTM method are as follows: a) not require any feature extraction, b) avoid using any handcrafted features, c) detect faults faster than the existing models, using the same data set and d) use smaller number of sensors to reduce the cost of operation of an offshore wind turbine. Based on the obtained results, we should remark that our data-driven approach can also be used in any time-domain data sets obtained from other sources. Even though the performance of our proposed ConvLSTM model is outstanding, there are some suggestions as follows for achieving better results.

- 1) Model uncertainty plays a significant role in enhancing the trustworthiness of the results obtained by the deep learning algorithms. However, using uncertainty quantification (UQ) methods in deep learning pose some challenges. In this study the UQ methods are not implemented and we believe that proposing a model with UQ methods can improve the performance of current model. Meanwhile, UQ methods can bring the results closer to reality.
- 2) Another issue in our proposed model is the final prediction step. The proposed model has only one prediction step while by having more predictions and using different models, the performance may improve. To deal with this issue, prediction-based fusion methods can improve the final results. In this regard, a novel weighted ensemble model that combine various deep learning methods is suggested.

Further recommendations for future research directions are also summarized as follows:

- 1) Work with real-world lower frequency data sets.
- 2) Use some hybrid models with different fusion approaches, either early or late fusion, and also employ ensemble leaning techniques.
- 3) Consider other faults including the system faults.
- 4) Reduce even further the number of sensors.

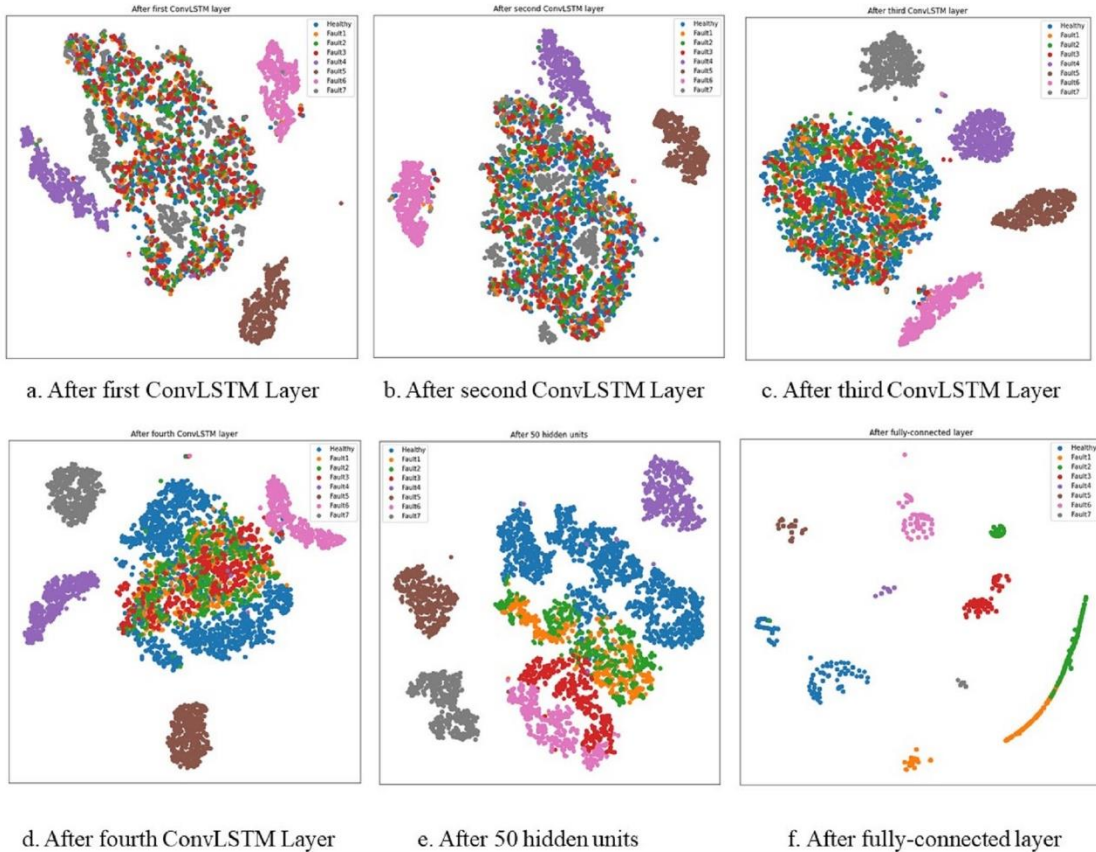


Fig. 6. The t-SNE representation of the feature distribution in ConvLSTM.

## REFERENCES

- [1] I. Goodfellow, Y. Bengio, and A. Courville, *Deep learning*. MIT Press, 2016.
- [2] W. Qiao and D. Lu, "A survey on wind turbine condition monitoring and fault diagnosis—Part I: Components and subsystems," *IEEE Trans. Ind. Electron.*, vol. 62, no. 10, pp. 6536–6545, 2015.
- [3] W. Qiao and D. Lu, "A survey on wind turbine condition monitoring and fault diagnosis—Part II: Signals and signal processing methods," *IEEE Trans. Ind. Electron.*, vol. 62, no. 10, pp. 6546–6557, 2015.
- [4] Z. Hameed, Y. S. Hong, Y. M. Cho, S. H. Ahn, and C. K. Song, "Condition monitoring and fault detection of wind turbines and related algorithms: A review," *Renew. Sustain. Energy Rev.*, vol. 13, no. 1, pp. 1–39, 2009.
- [5] M. Ruiz *et al.*, "Wind turbine fault detection and classification by means of image texture analysis," *Mech. Syst. Signal Process.*, vol. 107, pp. 149–167, 2018.
- [6] G. Jiang, P. Xie, H. He, and J. Yan, "Wind turbine fault detection using a denoising autoencoder with temporal information," *IEEE/ASME Trans. Mechatronics*, vol. 23, no. 1, pp. 89–100, 2017.
- [7] J. Lei, C. Liu, and D. Jiang, "Fault diagnosis of wind turbine based on long short-term memory networks," *Renew. Energy*, vol. 133, pp. 422–432, 2019.
- [8] Y. Si, L. Qian, B. Mao, and D. Zhang, "A data-driven approach for fault detection of offshore wind turbines using random forests," in *IECON 2017-43rd Annual Conference of the IEEE Industrial Electronics Society*, 2017, pp. 3149–3154.
- [9] V. Pashazadeh, F. R. Salmasi, and B. N. Araabi, "Data driven sensor and actuator fault detection and isolation in wind turbine using classifier fusion," *Renew. Energy*, vol. 116, pp. 99–106, 2018.
- [10] P. F. Odgaard, J. Stoustrup, and M. Kinnaert, "Fault-tolerant control of wind turbines: A benchmark model," *IEEE Trans. Control Syst. Technol.*, vol. 21, no. 4, pp. 1168–1182, 2013.
- [11] P. F. Odgaard and K. E. Johnson, "Wind turbine fault detection and fault tolerant control-an enhanced benchmark challenge," in *2013 American Control Conference*, 2013, pp. 4447–4452.
- [12] J. M. Jonkman and M. L. Buhl Jr. "FAST user's guide," *Natl. Renew. Energy Lab. Golden, CO, USA, Tech. Rep. No. NREL/EL-500-38230*, 2005.
- [13] J. Jonkman, S. Butterfield, W. Musial, and G. Scott, "Definition of a 5-MW reference wind turbine for offshore system development," *Natl. Renew. Energy Lab. Golden, CO, USA*, 2009.
- [14] B. J. Jonkman and L. Kilcher, "TurbSim user's guide: version 1.06.00," *Golden, CO, USA*, 2012.
- [15] D. S. Ochs, R. D. Miller, and W. N. White, "Simulation of electromechanical interactions of permanent-magnet direct-drive wind turbines using the fast aeroelastic simulator," *IEEE Trans. Sustain. Energy*, vol. 5, no. 1, pp. 2–9, 2013.
- [16] Y. Vidal, L. Acho, N. Luo, M. Zapateiro, and F. Pozo, "Power control design for variable-speed wind turbines," *Energies*, vol. 5, no. 8, pp. 3033–3050, 2012.
- [17] B. Beltran, T. Ahmed-Ali, and M. E. H. Benbouzid, "Sliding mode power control of variable-speed wind energy conversion systems," *IEEE Trans. Energy Convers.*, vol. 23, no. 2, pp. 551–558, 2008.
- [18] G. Borboudakis and I. Tsamardinos, "Forward-backward selection with early dropping," *J. Mach. Learn. Res.*, vol. 20, no. 1, pp. 276–314, 2019.
- [19] R. Chaaban, D. Ginsberg, and C.-P. Fritzen, "Structural load analysis of floating wind turbines under blade pitch system faults," in *Wind Turbine Control and Monitoring*, Springer, 2014, pp. 301–334.
- [20] J. Liniger, H. C. Pedersen, and M. Soltani, "Reliable fluid power pitch systems: A review of state of the art for design and reliability evaluation of fluid power systems," in *ASME/BATH 2015 Symposium on Fluid Power and Motion Control*, 2015.
- [21] L. Chen, F. Shi, and R. Patton, "Active FTC for hydraulic pitch system for an off-shore wind turbine," in *2013 Conference on Control and Fault-Tolerant Systems (SysTol)*, 2013, pp. 510–515.
- [22] A. Karpathy and F. F. Li, "Stanford CS class CS231n: convolutional neural networks for visual recognition," Spring 2019.
- [23] C. M. Bishop, *Pattern Recognition and Machine Learning*. Springer, 2006.
- [24] A. Karpathy and F. F. Li, "CS231n convolutional neural networks for visual recognition," *Neural Networks*, vol. 1, 2016.
- [25] S. Hochreiter and J. Schmidhuber, "Long short-term memory," *Neural Comput.*, vol. 9, no. 8, pp. 1735–1780, 1997.
- [26] K. Greff, *et al.* "LSTM: A search space odyssey," *IEEE Trans. Neural Net. and Learn. Syst.*, vol. 28, no. 10, pp. 2222–2232, 2016.
- [27] S. H. I. Xingjian, *et al.* , "Convolutional LSTM network: A machine learning approach for precipitation nowcasting," in *Advances in Neural Information Processing Systems*, 2015, pp. 802–810.
- [28] S. Ioffe and C. Szegedy, "Batch normalization: Accelerating deep network training by reducing internal covariate shift," *arXiv Prepr. arXiv1502.03167*, 2015.
- [29] D. P. Kingma and J. Ba, "Adam: A method for stochastic optimization," *arXiv Prepr. arXiv1412.6980*, 2014.
- [30] N. Ketkar, "Introduction to keras," in *Deep learning with Python*, Springer, 2017, pp. 97–111.
- [31] M. Abdar, U. R. Acharya, N. Sarrafzadegan, and V. Makarenkov, "NE-nu-SVC: A new nested ensemble clinical decision support system for effective diagnosis of coronary artery disease," *IEEE Access*, vol. 7, pp. 167605–167620, 2019.
- [32] M. Zomorodi-moghadam, M. Abdar, Z. Davarzani, X. Zhou, P. Plawiak, and U. R. Acharya, "Hybrid particle swarm optimization for rule discovery in the diagnosis of coronary artery disease," *Expert Syst.*, p. e12485, 2019.
- [33] M. Abdar and V. Makarenkov, "CWV-BANN-SVM ensemble learning classifier for an accurate diagnosis of breast cancer," *Measurement*, vol. 146, pp. 557–570, 2019.
- [34] T. Fawcett, "ROC graphs: Notes and practical considerations for researchers," *Mach. Learn.*, vol. 31, no. 1, pp. 1–38, 2004.
- [35] H. He and E. A. Garcia, "Learning from imbalanced data," *IEEE Trans. Knowl. Data Eng.*, vol. 21, no. 9, pp. 1263–1284, 2009.
- [36] L. van der Maaten and G. Hinton, "Visualizing data using t-SNE," *J. Mach. Learn. Res.*, vol. 9, no. Nov, pp. 2579–2605, 2008.



# Supplementary Material of: A Generalizable Model for Fault Detection in Offshore Wind Turbines Based on Deep Learning

Soorena Salari and Nasser Sadati, *Member, IEEE*

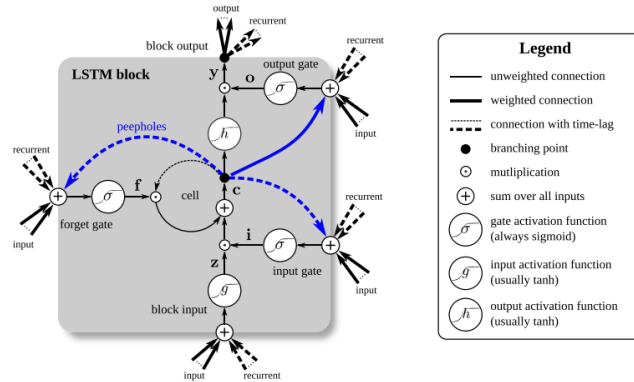


Fig. 1S. LSTM structure [1].

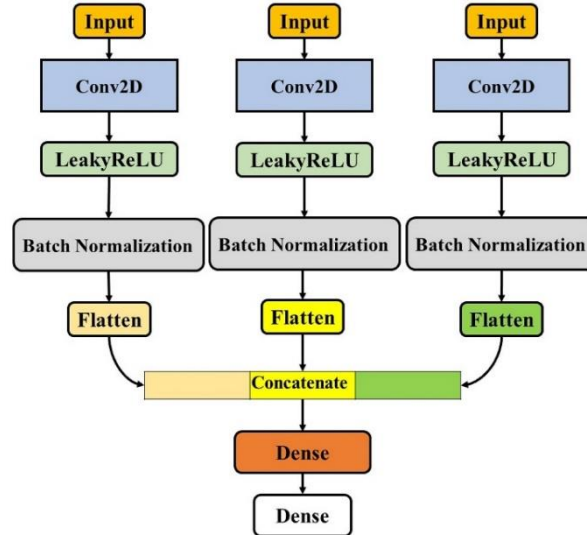


Fig. 2S. The first proposed CNN for fault detection.

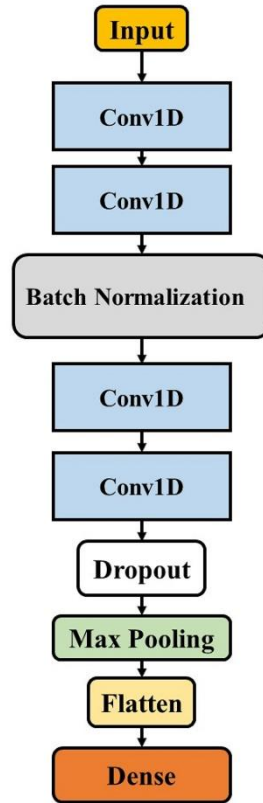


Fig. 3S. The second proposed CNN for fault detection.

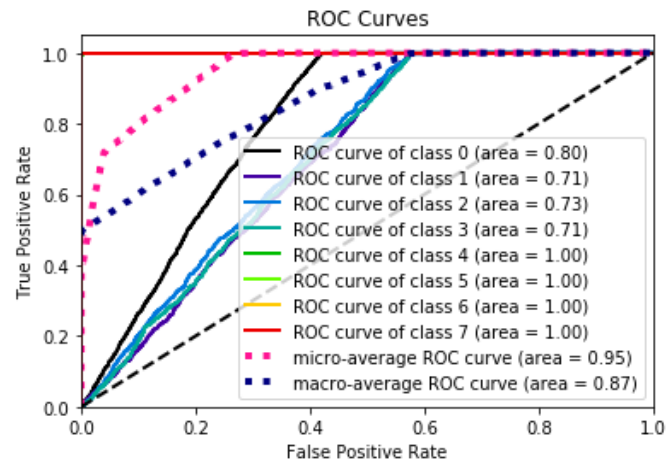


Fig. 4S. The ROC curve for the first CNN.

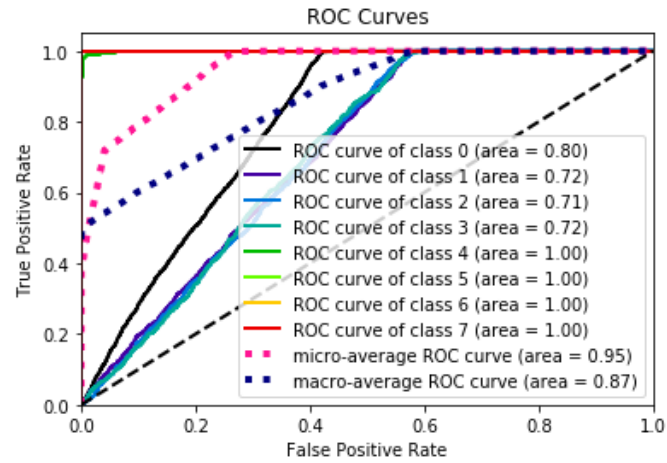


Fig. 5S. The ROC curve for the second CNN.

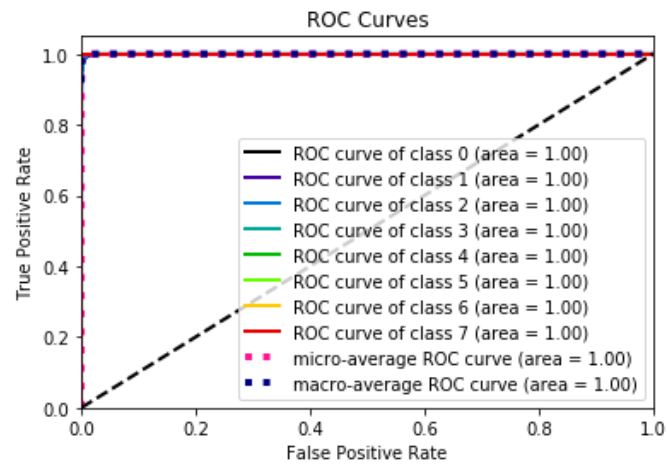


Fig. 6S. The ROC curve for the ConvLSTM.

## REFERENCES

- [1] K. Greff, et al. "LSTM: A search space odyssey," *IEEE Trans. Neural Net. and Learn. Syst.*, vol. 28, no. 10, pp. 2222–2232, 2016.